APPLIED ORGANOMETALLIC CHEMISTRY
Appl. Organometal. Chem. **13**, 399–418 (1999)

REVIEW

Sonogels and Derived Materials

Eduardo Blanco, Luis Esquivias, Rocío Litrán, Manuel Piñero, Milagrosa Ramírez-del-Solar and Nicolás de la Rosa-Fox
Dep. Física de la Materia Condensada, Universidad de Cádiz, Apartado 40, Puerto Real, 11510 Cádiz, Spain

Nowadays the sol–gel process is used by an increasing number of researchers for the preparation of various products, including bulk materials, films, membranes or fibers. The application of ultrasound (sonocatalysis) to the precursors gives rise to materials with new properties, known as sonogels. The absence of additional solvent and, mainly, the effects of ultrasonic cavitation create a unique environment for sol–gel reactions leading to particular features in the resulting gels: high density, fine texture, homogeneous structure etc. These properties determine the evolution of sonogels on further processing and the final material structure. In this sense, the full exploitation of sonocatalysis requires a thorough understanding of the processes involved and their sensitivity to reaction parameters. For this purpose, we have used diverse techniques to investigate the microstructural evolution during different steps in the sonogel process. The results of these studies are reported here. Finally, we present an overview of some applications for which the mechanical, textural and optical characteristics of sonogels are quite useful. Copyright © 1999 John Wiley & Sons, Ltd.

Keywords: sonogels, sol–gel process, xerogels, aerogels; ormosils; doping; ceramic composites

* Correspondence to: Luis Esquivias, Dep. Física de la Materia Condensad Universidad de Cádiz, Apartado 40, Puerto Real, 11510 Cádiz, Spain.

1 INTRODUCTION

1.1 Historical outline of sol–gel processing

In a strict sense, 'sol–gel processing' is the synthesis of an oxide network via inorganic polymerization starting from molecular precursors in solution. This term frequently is extended to refer to the preparation of inorganic oxides by 'wet chemistry'. The sol–gel process provides a new approach to the preparation of glasses and ceramics with many advantages over conventional methods. Pioneers[1,2] claimed that this technique was particularly suitable for the synthesis of complicated multicomponent glasses because the liquid state favors homogeneous mixing at temperatures much lower than the fusion point. In this way, in 1962 Schröder reported the preparation of vitreous layers of individual and mixed oxides (SiO_2, TiO_2 and others) by hydrolysis and polycondensation of metal alkoxides. Two years later Mackenzie[3] included the hydrolysis of metal alkoxides in his compilation of unconventional routes to glasses. This was a turning point for glass science when the term 'non-crystalline solid' began to be used to define a glass[3] instead of the operational 'product of fusion'. Until then, the definition of glass supposed a process that involved cooling from the melt. However, the first applied research on sol processes occurred in a field of heavy industry. In the 1968 IAEA (International Atomic Energy Agency) panel, Hardy[4] suggested that this process was particularly useful for manufacturing microspheres with closely controlled production, composition and density, appropriate to prepare substantial amounts of nuclear ceramic fuels. In the 1970 meeting of the same series, Wymer[5] gave a status report on sol–gel work for ceramic fuel production where seven large companies in the USA were involved in process development. At that time, there was a major reduction in sol–gel activity in

CCC 0268–2605/99/050399–20 $17.50

the USA because the administration stopped support of sol–gel processes for fast reactor fuels. However, the appearance of high-temperature gas-cooled reactors (HTGRs) on the market provided an incentive to conduct sol–gel work to prepare fuel microspheres. This application was the subject of deep discussion and development during the early 1970s[6] until the final cancellation of the nuclear fuel program. As fuel microsphere development work slowed down, sol–gel processing of thin dielectric coatings[1] became the only well-established application for sol–gel processing. This approach was developed at the end of the 1970s and extended to process advanced ceramic materials and glasses for technological applications.

Until the mid -1980s, gel-to-glass conversion was considered the most interesting technological application for sol–gel processing and received most attention and effort. If asked about future trends in sol–gel processing, not many scientists would have foreseen the research carried out at present in most sol–gel laboratories. The emphasis was on the chemical synthesis of materials at room temperature or slightly elevated temperatures and homogeneous multicomponent products of highly controlled purity. Since then, basic research resolved and explained the majority of the chemical and physical phenomena of sol–gel processing, and laid the foundations for a number of present and future applications. Currently, rheological properties of sols and gels are finding utility for preparing bulk products, films, membranes, fibers and composites[7–12]. Brinker and Scherer,[13] in their excellent treatise on *The Physics and Chemistry of Sol–Gel Processing*, have exhaustively described the possibilities for sol–gel methods for synthesizing a large number of preforms.

1.2 An insight into the sol–gel process

Avoiding any phenomenological definition or description, a gel is a two-phase medium composed of a solid and a fluid. The solid phase particles range in size from 1 to 100 nm.[14] Gels are often classified either as *particulate* or *polymeric*.[15,16] 'Particulate' means that the solid phase forms by aggregation of dense, non-polymeric particles. Particulate gels are obtained by destabilization of an aqueous colloidal solution of oxides, hydroxides or mineral salts. For this reason they are also called *hydrogels*. The term 'polymeric' is usually employed just for those gels obtained by polymerization of a metallo-organic compound in alcohol solution. *Alcogel* is another term often used to describe polymeric gels.

It is commonly asserted that a more attractive feature of sol–gel processing is the possibility of tailoring unique materials, especially by polymerization of a metallo-organic compound to a polymeric gel. The key is to design the proper monomer that will polymerize to form M–O–M structures. Metal alkoxides, $M(OR)_n$, fulfill these requirements, where M is the metal and R an alkyl radical. Popular choices used in the preparation of silica-based gels are tetramethoxysilane, $Si(OCH_3)_4$, and tetraethoxysilane, $Si(OC_2H_5)_4$, known as TMOS and TEOS, respectively. Since these compounds and water are not miscible, a common solvent (generally, methyl or ethyl alcohol) has to be added to obtain an initially homogeneous liquid. The chemical reactions involved are complicated but can be summarized by Equations [1] and [2].

Hydrolysis: $$M(OR)_n + nH_2O \rightarrow M(OH)_n + nR(OH) \quad [1]$$

Polycondensation: $$pM(OH)_n \rightarrow pMO_{n/2} + \frac{pn}{2}H_2O \quad [2]$$

Hydrolysis and polycondensation can be accelerated or slowed down by employing an appropriate acid or base catalyst. These processes proceed simultaneously and are generally incomplete. Depending on the amount of water present, hydrolysis may go to completion or stop while the metal is only partially hydrolyzed. In the case where several different cations are used to form mixed-oxide networks, a complexation step may be required initially. When the alkoxide precursors have different hydrolysis rates (e.g. Al or Ti with regard to Si), a prehydrolysis of the alkoxysilane is preferred.[7,13] After a complex sequence of polymerization, sol formation and gelation, a high-surface-area microporous gel constituted of small particles (≈2 nm), with a formula approximated by:

$$(MO)_x(M'O)_{x'}(OH)_y(OR)_z$$

is formed. OH and OR account for reaction byproducts that can resonably easily leave the system, yielding a complex three-dimensional oxide polymer –M–O–M′–O–M–which preconfigures the network of corresponding oxide glasses.

One of the main problems in the preparation of bulk materials is to avoid cracking of the gel during

drying, due to the stresses caused by the capillary forces associated with the gas–liquid interfaces. Fractures are initiated if these stress differences are greater than the tensile strength of the material. According to Laplace's formula (for a capillary of radius r and a liquid having a wetting angle θ) the capillary pressure Δp is given by Equation [3]:

$$\Delta p = \frac{2\gamma \cos\theta}{r} \qquad [3]$$

All actions on these parameters that tend to minimize the capillary pressure gradient and increase the mechanical strength of the network should enhance the probability of monolithic gel formation. The direct solution is to let the liquid evaporate at a very low rate. This strategy, although effective, is not practicable because of the long drying times required. It would take weeks, even months, to form a monolithic dried gel (xerogel). One alternative to accelerate drying is to add drying control chemical additives (DCCAs) that modify the surface tension of the interstitial liquids, allowing fast elimination of the unwanted residues. DCCAs are incorporated in the starting mixture before gelling and, after an adequate heat treatment, a crack-free xerogel results.[17] Formamide is one of the most common DCCAs used for drying silica gels. The action of the formamide in the gelling process starts in the liquid state by inducing, under acid-catalyzed conditions, a progressive increase of the solution pH with time. The mechanism that eliminates cracking is not yet well understood, although a few explanations are plausible. The hydrolysis reaction is generally faster and more complete under acidic conditions and the average condensation rate is maximized near pH 4. Consequently, formamide addition to acid-catalyzed systems should allow efficient hydrolysis followed by a rapid condensation when formamide hydrolysis provokes an increase of the solution pH. Therefore, one effect of formamide addition may be gel strengthening. Small-angle X-ray scattering (SAXS) was used to investigate the differences in structure and kinetics during aggregation of solutions with formamide. This technique measures the angular dependence of the intensity scattered by a sample with heterogeneous electron density. Monomer aggregation leads to clusters that can be described as statistical polymeric balls.[18] The texture of the solution at the gel transition becomes finer as the formamide content increases. The xerogel structure has been depicted as a hierarchy of several levels by means of models built up using the Monte Carlo calculations, on the basis of random close packing (RCP) premises.[19–22] The effect of formamide addition is a decrease in the average cluster size at the gel transition, suggesting that this additive enhances the nucleation of growing aggregates. These effects are consistent with observations that formamide increases the microhardness of wet gels and correspondingly the pore sizes of dried gels, while maintaining a narrow pore size distribution.[23] On the other hand, the high viscosity of formamide leads to formation of a formamide layer on the gel surface. This probably reduces the capillary pressure in two ways: (1) by forming a surface film, it reduces the contact angle; (2) because of its low vapor pressure it evaporates very slowly, providing a plasticizing effect that minimizes crack formation.

Either way, the most efficient way of neutralizing the undesired effects of surface tension is to suppress the liquid–vapor interface. This is achieved by treating the gel in an autoclave under supercritical conditions for the solvent, taking care that the path of the thermal treatment does not cross the equilibrium curve. This technique, initially developed by Kistler,[24] was applied by Nicolaon and Teichner[25] to gels obtained from metallorganic compounds. A systematic investigation design to optimize supercritical extraction conditions to produce monolithic aerogels was carried out at Montpellier.[26–29] Two different strategies can be used to bypass the critical point: (1) adding an extra volume of liquid in the autoclave and heating; (2) applying pressure using an inert gas before heating.[30] The resulting product is a gel with its pores filled with air, the source of the term *aerogel*. Aerogels are very porous and brittle materials. They are interesting products in themselves because of their very particular structure that, in some cases, can be described in terms of fractal geometry. A series of Proceedings has been published devoted exclusively to these very unusual materials.[31] They are extremely light, with densities as low as 0.01 g cm^{-3}, fulfilling the autosimilarity condition over one order of magnitude.[32] Aerogels are among the rare, true examples of fractal materials. Fricke has investigated and reviewed aerogels as engineering materials.[33–35] They have been successfully tested as transparent thermal insulation in solar architecture because of their low thermal conductivity and high optical transparency. On the other hand, the small index of refraction they display allows their use in Čerenkov counters for detection of relativistic particles with momenta not covered by compressed gases or liquids.

As mentioned above, ten years ago the central

idea of sol–gel processing was to circumvent the classical high-temperature technique of obtaining glasses by a room-temperature process. Nowadays, the technique is used to prepare zero-, one-, two- and three-dimensional advanced materials, both amorphous and crystalline, because its forming capacity is extremely varied. For example, Barringer and Fegley have reported the preparation of a number of binary-oxide ceramic powders by the sol–gel process,[36] which permits the preparation of ultrafine particulate forms. Sakka *et al.* have studied the rheological behavior and spinnability of sols, and have developed methods of spinning continuous ceramic fibers that cannot be obtained by other methods.[37,38] Brinker *et al.* have developed extensive experience in sol–gel coating, as reported in numerous articles and reviews.[13] However, special care has to be taken to control the porosity. This step, which has been studied in great detail,[7,12,39] consists of annealing the porous gel–glass at elevated temperature, resulting in a dense non-porous material.

2 SONOGELS

In 1984 Tarasevich[40] described an approach to sol–gel processing eliminating the use of additional solvent (alcohol) by exposing TEOS–water mixture to intense ultrasonic irradiation. Thereafter, the Zarzycki and Esquivias groups conducted extensive work to establish the practical consequences of this approach for the kinetic and textural characteristics of the so-called sonogels.[41] These studies encompasses numerous systems, including pure SiO_2,[19,42–51] SiO_2–P_2O_5,[43,52,53] SiO_2–TiO_2,[18,54–59] ZrO_2,[60,61] SiO_2–Al_2O_3–MgO[62,63] (cordierite) and ormosils (ORganically MOdified SILicates).[64–66] In addition, sonogels have also been used as passive matrices for SiO_2 particles,[51] Al_2O_3 or ZrO_2 particles and fibers,[62,67] or as active phase for quantum dots (CdS[68–70] and CdSe[71] nanocrystals), organic dyes,[72–76] or even proteins.[77]

Other approaches have been proposed as solventless routes for gel processing, such as preparation by vigorous magnetic stirring of the initial mixture,[78] hydrolysis of $SiCl_4$ vapor in a water bath,[79] hydrolysis of TEOS at high dilution followed by a quick-setting pH change,[80] hydrolysis in highly acid conditions[81] or in the presence of carboxylic acids.[82]

When sonogels are being prepared, hydrolysis is carried out by subjecting the initial mixture (alkoxide + acidified water) to ultrasonic waves in an open glass container. Ultrasonic waves (20 kHz) are generated by a high-power ultrasonic horn, by means of a 13 mm titanium tip driven by an electrostrictive device. The energy dose delivered to the system is set by the output power of the generator (15 W) and the time, providing an additional parameter for controlling the sol and gel properties.[19]

An alternative experimental setup involves an ultrasonic bath.[83] In these cases a much lower ultrasonic intensity is supplied to the reactants and, consequently, the resulting samples do not offer the characteristic sonogel features.

When the alkoxide–water mixture is exposed to ultrasonic irradiation it emulsifies and an atomization effect is seen wherein alcohol release is observed.[44,46] When high energies are used, the most relevant effects on the chemical reactions occur because of cavitation phenomena. Cavitation takes place due to collapse of vapor bubbles in the liquid subjected to ultrasonic waves, producing extreme pressures and hot spots.[84] Acoustic cavitation includes three discrete stages: nucleation, growth and implosive collapse of cavitating bubbles.[85] When ultrasonic waves are propagated through the liquid, cavitation bubbles form during the rarefaction phase if the negative pressure attained is sufficient to break down the liquid. However, microcavities usually form around solid particles or gas nuclei trapped in the liquid, lowering the cavitation threshold for breaking down the liquid. Two theories have been proposed, on the basis of resonant bubbles[86] and transient collapsing bubbles,[87,88] respectively. In either case, propagation of the pressure wave through the liquid causes the bubble radii to oscillate around some equilibrium size. The bubbles grow up in each cycle because of evaporation of the reactant. Once the bubbles reach a critical size they implode under the high-pressure phase. The rapid compression of gas produced leads to nearly adiabatic heating due to the low thermal transport, inducing extremely high local temperatures. It is in this step that reaction takes place in the gas phase inside the collapsing bubble.

In practice, we can see at this point that the liquid 'blows up' abruptly and its temperature increases drastically. This process coincides with the hydrolysis reaction break-out and the release of alcohol vapor which, in turn, promotes the subsequent condensation reaction. The time required to cause liquid 'boiling' establishes an energy dose threshold for sonosol generation, below which a two-

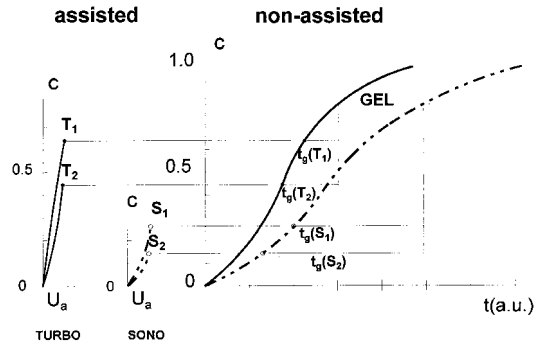

Figure 1 Influence of a change in the overall kinetic rate constants on the gelation time in sono (S_1 and S_2)- or turbo (T_1 and T_2)-assisted reactions. Subscripts 1 and 2 refer to two different sets of reaction conditions. The gelation time drops drastically when the assisted reaction is stopped before or after the solution reaches the inflection point in the curve of the polycondensed species concentration, *c(t)*.

phase mixture remains after sonication. The upper limit for the energy supply corresponds to the dose for which the reacting liquid gels in situ, i.e. in the container during sonication. The actual values for these limits are very dependent on the cavitation intensity reached and can be modified by varying the reacting system and conditions.[89,90] In consequence, the alkoxide type, pH, water concentration, presence of a DCCA, static ambient temperature, container diameter, degree of tip immersion and other parameters should be controlled to obtain reproducible results.

The first outstanding effect of ultrasound on the gelation process is the drastic decrease in the gelation time in comparison with the classic techniques, but obtained in the presence of alcohol. At constant temperature, the time for gelation decreases with increasing ultrasonic dose. Experimental curves show two decay regimes separated by an energy level that varies from 400 to 600 J cm^{-3} for the different systems, corresponding to predomination by hydrolysis and polycondensation, respectively.

A comparison of ultrasonic processing (sono-) with ultrarapid stirring (turbo-) methods has been undertaken.[46] A high-speed rotary blender (Ultraturrax TP 18/10) operating at 20000 rpm induces a higher temperature increase during reaction in TEOS–water mixtures. Foaming occurs during agitation once the threshold energy is surpassed. The resulting homogeneous solution gels after a period of time which, as for sonogels, depends exponentially on the energy dose supplied. Studies on the gelation time of both solventless routes seem to indicate that the rotary blender action induces a higher overall rate constant than ultrasound, giving rise to a highly polycondensed solution. By contrast, the overall kinetic rate constant of the turbosolution, once it is left on its own (after external agent action), is lower than that of the sonosolution. By using a simple model of the polycondensation ratio (the product of a second-order consecutive reaction,[91,92] the diverse influence of the reaction conditions on both sets of sols can be explained. Figure 1 is a plot of the evolution of the concentration of the polycondensed species *c(t)* during the whole process. Once the irradiation or stirring (assisted reaction) ceases, the system follows the typical path[91] for this kind of reaction (non-assisted) from the point corresponding to the degree of condensation reached, which determines the gelation time. Then, by changing conditions we modify the overall kinetic rate constants during the assisted reaction and, consequently, the gelation time (Fig. 1). According to this model, the turbosolution is more sensitive to the external agent, because the greater the rate constants, the greater the slope dc/dU_a and the higher polycondensation ratio reached during the assisted step. Once the threshold energy for foaming, *c(t)*, has passed the inflection point, the gelation time decreases sharply. The reaction conditions for high-speed stirring action to allow to reach that point in less time than sono-catalysis for the same amount of energy furnished to the system.[46]

Dynamic calorimetric experiments on the kinetics of the ultrasound-assisted acid hydrolysis of TEOS confirm that the release of alcohol during solventless reaction enhances further reaction through a parallel autocatalytic path.[93] On the basis of these results, Vollet *et al.*[94] have proposed a kinetic model based on a dissolution and reaction mechanism in which ultrasound forces the initial dissolution for the onset of reaction. The alcohol produced during the initial reaction favors further dissolution.

Zarzycki[49] has investigated the elastic and viscoelastic properties of sonogels to identify any changes in the initial crosslinked state of reticulation induced by ultrasound. The elastic moduli of samples increase with time because of extended crosslinking and syneresis effects until a certain value (in the range of 10^5–10^7 Pa, depending on the sample) is achieved. The effect of the ultrasonic dose is to raise this limiting level attained. In contrast, the fracture surface energy, Γ, tends, for a large elastic modulus, toward the same constant

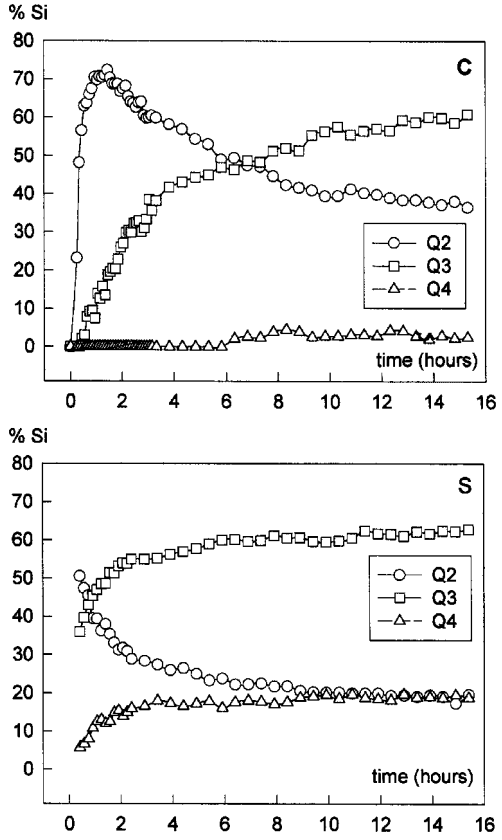

Figure 2 Evolution, as a function of time, of the relative concentrations deduced from the NMR peak intensities of the condensed species: C, classic sol; S, sonosol.

value (0.025 ± 0.01 J m^{-2}) independently of the ultrasonic dose. Zarzycki found a different behavior for uniaxial relaxation times. This revealed that a higher crosslink density state was obtained after longer radiation times for sonogels, which progress further on aging.

3 SONOGEL STRUCTURE

3.1 Local probes

3.1.1 From sol to gel

We have used nuclear magnetic resonance (NMR) spectroscopy of ^{29}Si to monitor the states of bridging groups (SiO_4)[95] during gelation by sonochemical and classic methods. Figure 2 shows the concentration of species Q_n as a function of time, where n is the number of bridging oxygens in a (SiO_4) [95] group. After 20 minutes of sonication, the sonosol consisted of 42% of network-forming species ($Q_3 + Q_4$), whereas in the corresponding classic sol only 10% of the species were Q_3 and Q_4. The Q_4 concentration in the sonogel reached 20% 8 h after initiation of sonication. This contrasts with 3% in the classic route for the same time after preparation (Fig. 2).[96] In terms of reaction mechanism this means, as basic 'sonocatalysis' promotes hydrolysis.[46] The concentration of silanol groups is higher and consequently the rate of bridging-O formation is also higher.

^{31}P NMR was used as an additional tool to investigate the effects of ultrasonic mixing on the structure of SiO_2–P_2O_5 gels. When tetraethyl phosphate (TEP) was used as a P precursor, the spectra (both classic and sono-) consisted of a set of seven peaks centered at 1 ppm. Such a spectrum is characteristic of the phosphate triester, indicating that TEP is not hydrolyzed in these conditions.

TEP with the stoichiometrically required amount of water was subjected to ultrasound and, by monitoring its evolution by Raman spectroscopy, found to be non-reactive. One month after the beginning of the reaction, no evolution of the bands was observed.

3.1.2 Xerogels and aerogels

We have combined ^{29}Si MAS-NMR and wide-

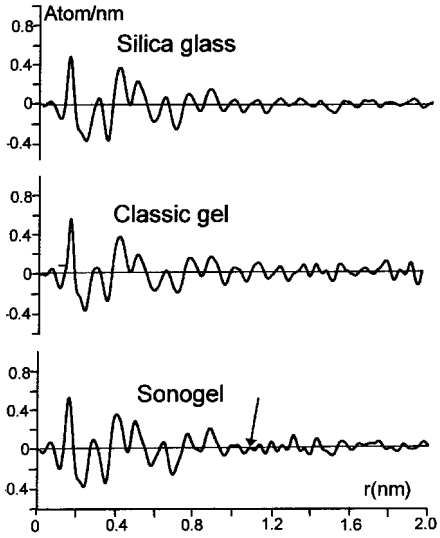

Figure 3 Reduced RDFs of sono- and classic gels: The arrow indicates where the curve oscillations start to differ from those of the silica glass RDF, included for comparison.

angle X-ray scattering (WAXS) to conduct studies on the structure of dried sonogels. The average number of atoms per unit length situated at a distance r from an arbitrary atom taken as a reference is given by the radial distribution function $RDF(r) = 4\pi r^2 \rho\ (r)$, where $\rho\ (r)$ is the local atomic density. The first peak position of the RDF indicates the most probable distance of the first neighbors. In Fig. 3 the reduced RDFs are represented for a sonogel, a classic gel and silica glass. These values represent the deviation of the RDFs from a uniform distribution $4\pi r^2 \rho_0$, where ρ_0 is the macroscopic density. The average bond length was found to be 0.164 ± 0.001 nm both for sonogels and classic gels, 0.002 nm longer than in vitreous silica. The average atom coordination in silica sonogels is very near that of the bulk silica glass. Figure 3 shows another important finding: there is a correspondence between sonogel and silica bulk glass RDF maxima up to r near 1.1–1.2 nm. Beyond this distance the sonogel curve deviates sharply. In the case of the classic gel the deviation occurs more gradually. These differences were interpreted to mean that sonogels are formed by monosized elementary particles of $\sim$1 nm radius, whereas the classic gel is formed of particles with a wide size distribution.

The skeletal density of the solid phase was calculated from the RDF(r). This was evaluated by the maximum-entropy method.[97] The RDF was found to be compatible with the experimental data and, in particular, with the solid backbone density. The macroscopic atomic density of both the sonogel and the classic silica aerogel was found to be $\rho_0 = 63.0 \pm 0.5$ atom nm^{-3} (2.09 ± 0.02 g cm^{-3}) and the density of pure silica glass, used as a reference, was $\rho_0 = 66.0 \pm 0.5$ atom nm^{-3} (2.19 ± 0.02 g cm^{-3}). These differences come from the presence of non-bridging oxygens (NBOs) on the pore–matrix interface in the aerogels, causing lengthening of the average Si–O bonds.[98]

A first approximation to the number of NBOs was made from the area beneath the first RDF peak, A. This is related to the average number of atoms in the first coordination sphere by Equation [4]:

$$A = \frac{1}{\left(\sum x_x Z_i\right)^2} \sum \sum x_x Z_i Z_j n_{ij} \qquad [4]$$

where Z_i is the i-element atomic number; n_{ij} is the average number of j-type atoms in the first coordination sphere of a j-type atom, calculated from a hypothetical assumption which this case is that each atom has its bonds satisfied except for a fraction α of O, $0 < \alpha < 1$, i.e. $n_{11} = n_{22} = 0$, $n_{12} = 4$ and $n_{21} = 2 - \alpha$, giving $A = 2.99 - 0.747\alpha$. This expression for A was compared with the experimental values $A_{sono} = 2.97 \pm 0.10$ and $A_{classic} = 2.87 \pm 0.10$, giving values of $NBO_{sono} \cong 8\%$ and $NBO_{classic} \cong 16\%$. According to these values, the sonogel atomic network is more reticulated than classic gels. The sonogel route gives an atomic short-range order close to that of the bulk silica glass.

These results support the ^{29}Si MAS-NMR results that indicate that the sonogel structure is more crosslinked than gels obtained in alcoholic solution. However, the OH surface coverage calculated assuming a model of non-contacting spherical particles of 1 nm BET radius is several times higher than calculated from N_2 physisorption measurements. This was interpreted as indicating that an important number of OH groups are buried in the sonogel structure.[50] These hydroxyl groups are difficult to eliminate, causing difficulties when full densification to form a glass is intended.

In ^{31}P NMR of SiO_2–P_2O_5 we denote by Q'^n a phosphate bound to n silicon atoms through P–O–Si bonds. Only the peaks Q'^0 and Q'^1 of sono-aerogels with P/Si = 0.1:1 are observed just after supercritical drying. For higher temperatures, the species Q'^2 and Q'^3 appear. However, a large number of species Q'^0 and Q'^1 remain, even at temperature higher than 1140 °C, indicating that the average connectivity of PO_4 remains low. For larger ratios (P/Si = 0.85:1) the peak Q'^0 can be seen even without magic-angle spinning. This fact indicates the presence of quasi-liquid species with free rotation that have not reacted with silica during this step in the process. After drying, all ^{29}Si MAS-NMRs of aerogel give a single broad peak at the position characteristic of Q^4 Si species, where the silicate tetrahedra are coordinated to four other silicon atoms. Increasing the heat-treatment temperature causes an increase in the number of P–O–S in the glass. However, above 500 °C, characteristic peaks of the Si-5-$(PO_4)_6$ crystalline phase appear.

The other binary system studied was SiO_2–TiO_2. The local order around the Ti atoms in 5 mol% titania-doped silica aerogel was investigated by X-ray absorption.[59] The Ti coordination is slightly affected by the method of preparation. Most of Ti atoms are six-coordinated forming very distorted tetrahedra, with loose bonds. For Ti/Si = 0.05:1 the sonogel route gives a less disordered network than the classic one, presenting a network structure close to that of the bulk glass. However the distribution of

Ti atoms does not correspond to a perfect statistical distribution but rather possesses domains where the Ti atoms are especially abundant.

3.2 SAXS

The growth kinetics of pure silica sono- and classic networks before gelation was monitored by SAXS using the LURE synchrotron facility at Orsay (France). The basic theory behind this technique is as follows.

The scattered intensities (I) are given as a function of the scattering vector modulus q. Its physical meaning is the momentum transfer from the incident to scattered waves. I and the density distribution in real space are related through a Fourier transform. Measuring the scattered intensity at momentum transfer q is equivalent to analyzing the real-space density distribution with a resolution $2\pi/q$.

In a standard ln *I(q)* versus ln q plot, three regions can be observed:

(a) *Guinier region:* Corresponds to very low where ln *I(q)* is almost constant. The analysis can be approximated by Guinier's law,[100] which provides information about the overall size of scatterers:

$$I(q) = I(0)\exp\left(-\frac{{R_g}^2 q^2}{3}\right) \qquad [5]$$

where $I(0)$ is the intensity at $q = 0$ and R_g is the gyration radius of the aggregates. R_g is calculated from the linear regression in a log *I(q)* versus q^2 plot (Guinier's plot). In dilute systems, R_g gives the characteristic particle size. If the system is dense, it gives a correlation length above which the system can be considered homogeneous. The Guinier's plot also provides, by extrapolation, $I(0)$ from which a correlation volume,

$$V_C = 2\pi^2 I(0)/Q_0 \qquad [6]$$

is calculated. This is a geometrical parameter related to the average volume of the scattering centers, Q_0, where $Q_0 = \int_0^{00} I(q)q^2\,dq$. This is known as Porod's invariant and is independent of the scatterer's geometrical shape. If we assume a spherical geometry for this volume, a correlation radius can be estimated.

When the q interval to which Equation [5] applies is narrow for a reliable linear regression, a good agreement is obtained with Zimm's approximation:[101]

$$\frac{1}{I(q)} = \frac{1}{I(0)}\left(1 + \frac{q^2 {R_g}^2}{3}\right) \qquad [7]$$

suitable for $qR_g \approx 1$ if the particle shape is known.

(b) *Fractal region:* For $1/R_g < q < 1/a$, where a is the elementary particle size. *I(q)* exhibits a potential dependence,[102] $I \propto q^{-x}$, over one order of magnitude. This means that the material has a mass fractal of dimension $D = x$ which can be calculated from the slope of a log I versus log q plot.

(c) *Porod's region:* For q large enough, *I(q)* tends progressively to a q^{-4} dependence when the particles are smooth with a well-defined interface. In the case of a surface fractality being present, behavior intermediate between (b) and (c) can be observed. The slope of the log I versus log q plot would be $-2D + D_s$, where D_s is the surface fractal dimension.

Porod's limiting law states that

$$\lim(q^4 I(q)) \rightarrow \frac{S}{V}\frac{Q_0}{\pi} \qquad [8]$$

where S is the surface area and V the volume of the particles. In the case of a dense system this relationship gives an estimate of the specific surface S/V of the system.

Between these regions, a progressive transition is observed, called a crossover. Thus, $q = q_M \approx 1/R_g$ is the crossover between Guinier and fractal scattering. The position q_m of the crossover between the fractal and Porod's regions defines the size $R' = 1/q_m$ of the primary particles which comprise the fractal aggregates.

From sol to gel

Curves in Fig. 4 (a) and (b) are representative sets of the aggregation state for different times. Close to the gel point ($t/t_G \approx 1$) the curves are consistent with a q power-law which increases with time. The limiting slopes are $D_{sono} = 1.77$ and $D_{classic} = 1.97$ with $R' \approx 0.25$ nm in the sono sample. The crossover with Porod's region in the classic case is beyond the upper limit of the measured q interval. Slopes more positive than -2 are attributed to a mass fractal behavior, with slightly branched but very entangled growing aggregates.[105] However, the linearity of the sonogel plot of log I versus log q

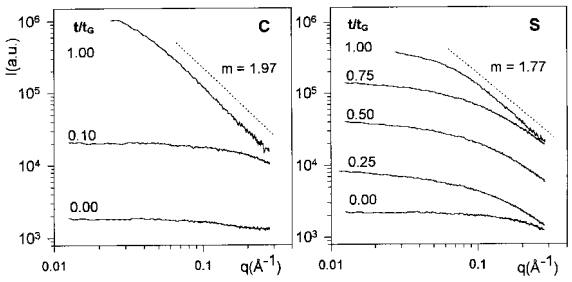

Figure 4 Development of the scattering profiles for sono- and classic TiO_2–SiO_2 sols: t_g is the gelation time. (Curves have been vertically displaced the same relative distance for clarity.).

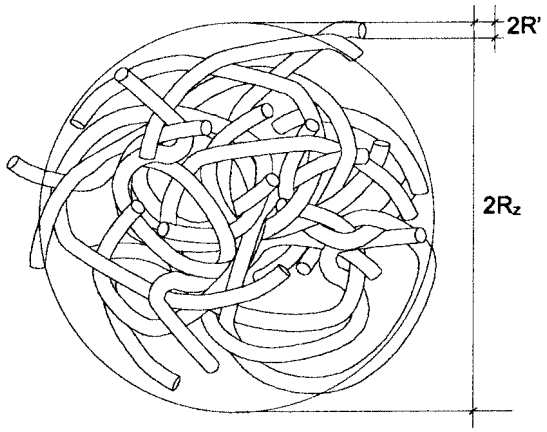

Figure 6 Schematic illustration of the proposed model.

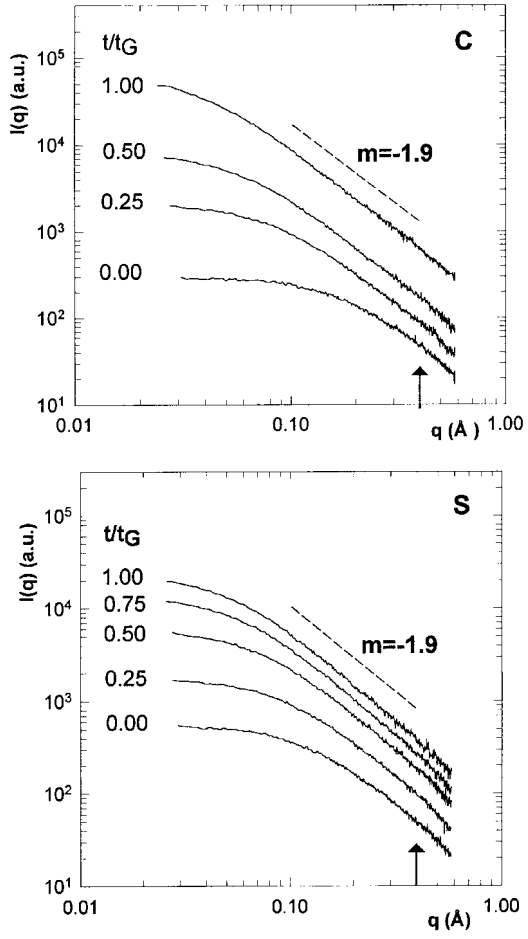

Figure 5 Development of the scattering profiles for C (classic) and S (sono-) silica sols: t_g is the gelation time. (Curves have been vertically displaced the same relative distance for clarity.).

is not extensive enough to assign a mass fractal structure in a strict sense. No evolution with time for the *S/V* ratios of the scatterers (Eqn [8]) was observed. On the basis of these findings, the internal structure can be described as consisting of rod-like scatterers that grow with an essentially constant section.

For $t = t_G$, R_g of the pure silica sonogel (1.6 nm), can be calculated from Equation [7]. There are two characteristic correlation lengths (R_g and R'), from which we proposed a model of statistical balls or polymeric clusters.[54,103] For $t = t_G$ R_g is almost four times smaller than that of the classic one (5.7 nm). The linear region domain in a log *I* versus log *q* plot for the classic gel is wider than for the sonogel. The classic gel is fractal because such a domain extends over more than one order of magnitude. In structural terms this means that the classic gel is less homogeneous and has a wider pore distribution than its sonogel counterpart. Its R', undetermined, is in any case smaller than that of the sonogel.

As has been mentioned already, one of the main problems in preparing homogeneous multicomponent gels arises when the precursors exhibit very different reaction rates. This causes the formation of a large number of M–O–M bonds, to the detriment of the number of M–O–M′ bonds, as in TiO_2–SiO_2, for instance. When preparing these systems a chelating agent (e.g. acetic acid) can be added to lower the hydrolytic reactivity of the Ti.[104] This method was combined with the application of ultrasound to promote hydrolysis of silicon alkoxides, before mixing the two precursors. The slope of the log *I* versus log *q* plot is ~1.9 from the early stage of gel formation (Fig. 5). This indicates that the local geometric structure, consisting of poly-

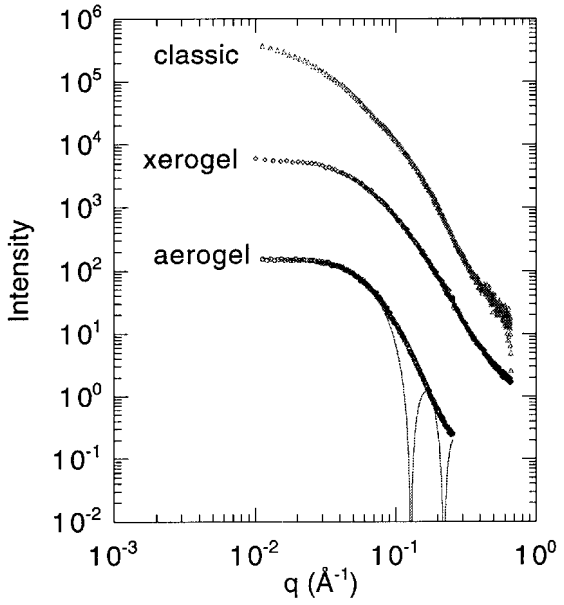

Figure 7 SAXS log–log curves for a sono-xerogel and -aerogel as well as for a classic aerogel. The bottom curve corresponds to the scattered intensity from a sphere of 3 nm radius.

meric clusters,[105] is unchanged during the sol–gel transition. The radius R_g deduced from Zimm's equation indicates that application of ultrasound reduces the size of the clusters as in the case of pure silica, as we have shown above.

The addition of Ti to a silica sol magnifies the structural effects induced by the ultrasound, i.e. the formation of small statistical balls. We have proposed a tentative model for the growing clusters, which is consistent with the structural considerations described above (Fig. 6). In such polymeric clusters, the cross dimension, R', of the elementary particles (or voids) remains unchanged, at least until gelation, while there is aggregation due to their lengthening which generates clusters of increasing size, R_g. This is evident from the shift toward lower q of the crossover between Guinier and fractal regions.

3.2.2 Xerogels and aerogels

The solid backbone and pore structure have been studied over a wide range of length: scales using small-angle X-ray scattering (SAXS) and gas physisorption (BET method). The wide plateau presented by the log *I(Q)* versus log *Q* curves of a SAXS experiment for sonogel samples (Fig. 7) reveals a homogeneous distribution of the silica aggregates and, hence, a well-defined radius of gyration. In the case represented in Fig. 7, Guinier's law gives R_g = 2.8 and 2.6 nm for the sono-aerogel and sono-xerogel, respectively. In the low q region where Guinier's law applies, the classic gel shows an increase in the scattered intensity produced by large aggregates with an 8.2 nm radius of gyration. The scattering intensity from a sphere of 3.0 nm radius is also represented to emphasize the near-spherical particles that form in sonogels. The continuous gel network avoids the appearance of discontinuities of the Bessel function at $qR = \tan(qR)$ values.

Particles of 2.4 and 2.2 nm radius were obtained from Equation [6] for the sono-aerogel and the sono-xerogel, respectively, whereas a value of 4.2 nm was obtained for the classic gel (Fig. 7).

Thus, as noted above, a SAXS study during gelation shows that the sonogel structure is coherent with a model of statistical balls.[18] These tangles of gel compact during aging, giving rise (after drying) to a very homogeneously packed aggregate formed from ~1 nm spheroid particles (see section 3.1.2). The value of q at which the curve begins to fall from the wide plateau in Fig. 7 indicates the size of the aggregates (~4–5 nm). Consequently, sonogels have a very narrow pore size distribution and a very high bulk density and surface/volume ratio, two or three times higher than gels prepared in alcohol solutions. Their very fine and uniform porosity and high apparent density, besides the short gelation time, are unique features of sonogels. These parameters are very sensitive to the ultrasonic dose supplied. The larger the dose, the finer the porosity and the higher the homogeneity. The gelling temperature also affects them in the same way. Porod's law (Eqn. [8])[100] applies to both sonogels and classic gels; it states that $I(q) \propto q^{-4}$ in the high-q region when the pore–solid matrix interface is sharp.

To elucidate the structure of these sonogels, we studied their sintering behavior. Gels sinter by a viscous flow mechanism, causing either pore collapse or coalescence of solid particles. The driving force for this process is supplied by interfacial energy, which allows sintering at low temperatures. The textural parameters of the changing gel structure can be monitored during the successive processing stages, which creates possibilities for tailoring structures for specific applications. The increase in the relative density parallels the decreases in specific surface areas, which supply the necessary energy for the viscous flow (Fig. 8).

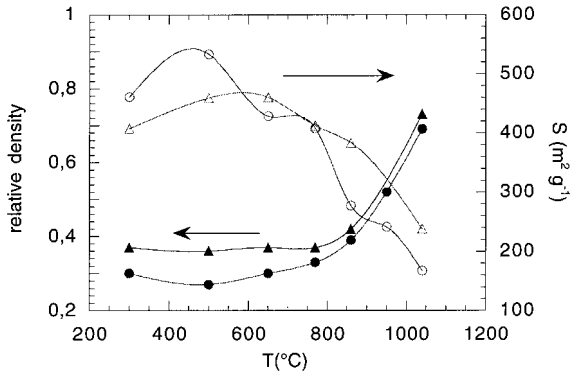

Figure 8 Relative density and specific surface area during the sintering process.

Analysis of the data indicates that the gel pore size distribution is spread over a few orders of magnitude and, accordingly, the densities depend strongly on the scale. The smallest length scale concerns the atomic density that can be calculated from WAXS data, as discussed above. A first level is given by SAXS data with nanoscale resolution, accounting for the arrangement of the elementary particles. Nitrogen physisorption resolves on the $\sim 10^2$ nm scale formed by clusters of these sphere-like particles (level 2). The third level of resolution we consider here describes the sonogel macroscopic structure. Each level can be monitored during sintering as a function of the packing fraction (Φ_i), defined as the relative density at consecutive levels. The experimentally determined packing fractions for each level are presented in Fig. 9 for sonogels prepared with high and low ultrasonic doses. The behavior at the nanoscale level, Φ_1, shows the existence of closed porosity that is not seen at the second level, Φ_2, by gas adsorption. From these results, one can conclude that sintering is easier with the high-ultrasonic-dose sonogels.

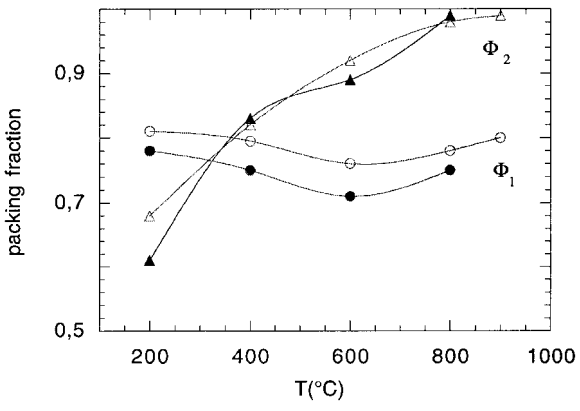

Figure 9 Evolution of the packing fraction during sintering of silica sono-aerogels prepared with high (open symbols) and low (solid symbols) ultrasonic doses.

The pore size distributions in sonogels are strongly influenced by DCCA.[23,48]. Thus, supercritically dried sonogels have pore size distributions with maxima at $r = 4.5$ nm, whereas those prepared with formamide have a narrower distribution with $r < 2$ nm. Another notable characteristic is that DCCA aging is faster and the asymptotic limiting value of the elastic modulus is higher than in the absence of DCCA (formamide) agents.

4 DERIVED MATERIALS

4.1 Hybrid organic–inorganic materials from sonogels

One of the more relevant features of the sol–gel process is the low temperature required. This offers a huge number of possibilities in the field of organic–inorganic composites.[106–111] One proposed route to these materials[112] incorporating an organic phase in the inorganic precursor sol, in combination with the sonogelation of these systems, has been described by several authors. When both phases bond chemically[113–115] a sono-ormosil[41] (also called a hard ormosil[66]) results after gelation, while purely physical interactions between the two phases[116,117] lead to an organic-doped sonogel.

4.1.1 Sono-ormosils

The preparation and properties of sono-ormosils were first investigated by Mackenzie's group.[64–66] As in inorganic sonogels, kinetic studies were carried out to elucidate the influence of ultrasound on the reactions involved. Once sonocatalysis starts, the reacting liquid temperature follows a path similar to that observed for simple sonogels, with a sharp increase to a plateau at 78 °C, probably due to the evaporation of ethanol produced by the hydrolysis. The gelation time is also reduced by ultrasound with a dependence on the energy applied, i.e. radiation time, which exhibits the typical crossover around 450 J cm^{-3}.[65]

Table 1. Textural parameters of hybrid samples heated at 100 °C.

DMS (molar%)	Bulk density ($g\,cm^{-3}$)	Skeletal density ($g\,cm^{-3}$)	S_{BET} ($m^2\,g^{-1}$)	V_p ($cm^3\,g^{-1}$)
24	1.39	1.45	350	0.20
40	1.14	1.32	372	0.27
55	1.07	1.18	220	0.24
65	~1.17	1.17	—	0.18

Ultrasound-assisted reactions carried out for different irradiation times have been monitored by NMR.[65,66]. The spectra reveal that hydrolysis and condensation of TEOS take place within several minutes of irradiation and further condensation occurs as time passes. Once the energy supplied has surpassed the inflection point, the intensity of the Q_3 and Q_4 peaks level off and a new peak, corresponding to copolymerization between the two precursors, starts to appear.

As with inorganic gels, the final properties of the ormosils are affected by ultrasound irradiation. They are denser and less porous, with better thermal stability too, than the ones prepared by the classic procedure.

Specific surface areas lower than $1\,m^2\,g^{-1}$ have been measured[65] on samples of the so-called hard ormosils that have been dried at 150 °C for 24 h to remove all the residuals from the pores. However, it has been shown[118] that if these hybrid samples are heated at 100 °C their pore size distribution and volume are strongly modified with respect to non-heat-treated samples. Our experiments on nitrogen adsorption on sono-ormosil samples, previously evacuated at 60 °C, show an enlargement of the pores with increasing organic content as well as a decrease in surface areas which can range to hundreds of square meter per gram (Table 1.)

One of the most interesting features of ormosils is the rubber-like behavior that samples with high PDMS content (>10%) exhibit.[115,119] Certainly, the mechanical properties of these materials have attracted considerable attention. In this respect, the increased density of sono-ormosils can enhance mechanical properties such as hardness.[66]

When compared with other materials, sono-ormosils are very much harder than the hardest organic plastics with Vickers hardness values close to those of soft glasses ($\sim 180\,kg\,mm^{-2}$). By considering only chemical bonds, Iwamoto and Mackenzie[66] developed a theoretical model for calculating the Vickers hardness and elastic modulus as related to the packing density, the dissociation energy per unit volume and the relative bond strength. Calculated values agree well with the experimental values obtained for the TEOS/PDMS systems and 30 mol% TiO_2-containing sono-ormosils, both prepared with isopropanol as solvent and with low organic content. From this model, higher elastic moduli and Vickers hardnesses are predicted for Al_2O_3- and ZrO_2-based systems, but these also present additional processing difficulties.

We have examined the dynamic elastic behavior of sono-ormosils as a function of the structural features by using Brillouin scattering.[120,121] From the measured dynamic and static hypersonic properties, the elastic constant c_{11} and the related hypersonic attenuation Γ were inferred. Calculated values range from 1 to 17 GPa. Refraction indices of sono-ormosils were also obtained from the Brillouin frequencies corresponding to the $\pi/2$ rad and backscattering geometries. All three parameters exhibit a behavioral changes when the monomer (DMS) molar ratio reaches a defined value, close to 50 mol%. This fact pointed to the existence of two different PDMS morphologies in the samples: segment-like and quasi-globular (liquid-like) forms, as clearly seen by NMR studies of dried samples. On this basis, we proposed a simple microstructural model, assuming these two different microstructures, the first one within the backbone of the sonogel network and the second one as a segregated phase for high DMS concentrations. Following Mackenzie's scheme,[115] both forms can be considered parallel-branched while being branched in series to the silica structure. Based on the assumed microstructure, a mathematical expression for the ormosil elastic constant is given by Equation [9]:

$$c_{11} = \left(\frac{1-x}{c_1} + \frac{x}{c_2(1-x) + c_3 x} \right)^{-1} \qquad [9]$$

where x is the DMS molar fraction and c_i are the elastic constants of the three phases involved. For the globular-like configuration, the elastic constant

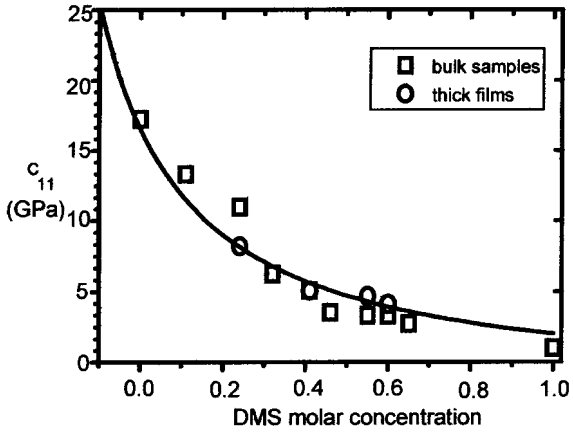

Figure 10 DMS concentration dependence of the longitudinal elastic constant calculated from Brillouin spectra. The line corresponds to the best fit to the proposed model.

of liquid PDMS is assumed ($c_3 = 1.018$ GPa). Fitting this model with the experimental values gives an estimate of the elastic constant for the sonogel ($c_1 = 17 \pm 2$ GPa) and for the segment-like PDMS ($c_2 = 3 \pm 1$ GPa) (Fig. 10).

4.1.2 Organic-doped sonogels

Ultrasonic cavitation has also been applied to the preparation of the aforementioned second type of hybrid materials. For effective entrapment of organic molecules, a stable and transparent sol–gel matrix is required with a narrow pore size distribution. This minimizes light dispersion effects and induces an uniform cluster size distribution of the guest.[117] In this way, several organic dyes were effectively trapped in the sono-xerogel pores, by adding the optically active phase in the sol step, leading to very stable composites for optical applications.[72,73,122,123] The most promising results were obtained by encapsulating copper phthalocyanine (CuPc). CuPc is a macrocyclic planar molecule with extended π-electron delocalization that gives rise to extremely large molecular second-order hyperpolarizabilities causing third-order non-linear optics processes.[124]

The effectiveness of the proposed route for trapping this molecular phase (CuPc) in a sonogel was examined by UV–Vis absorption at different stages of processing, from the starting sol to the dried composite.[73] The typical Q absorption band is broad and split with two maxima at 692 and 614 nm in all the curves. The band position and width indicate the coexistence of monomeric and aggregated species. In contrast, the increase in composite optical density with time, due to the higher Pc concentration in the shrinking inorganic network, implies effective molecule trapping in the host matrix. The absorption spectra of leachable liquids do not show any evidence of the Pc-Q band.

The non-linear optical behavior of the encapsulated molecules has been checked by various tests. The distortion of a 532 nm Nd:YAG laser beam profile after propagation through samples was analyzed and Fig. 11 is an example of the transmitted profiles obtained. Strong self-defocusing effects appear in samples with CuPc concentrations between 10^{-5} and 10^{-4} M,[74,75] revealing an intensity-dependent refractive index for the doped sonogels. These results show, in general, good agreement with theoretical predictions based on the Huygens–Fresnel formalism.[74] By fitting the theoretical expressions to the experimental profiles, we found very high-magnitude third-order susceptibilities that are not solely attributable to molecule–matrix interaction enhancement of the non-linear behavior. In fact, the relatively large time constant (87 ms) characterizing the exponential decay obtained in time-resolved experiments indicates that other non-electronic mechanisms contribute to the intensity dependence of the refractive index. However, the third-harmonic generation (THG) effect confirmed that electronic mechanisms also contribute to the total susceptibility.[76] From Maker-fringes analysis[125] similar $\chi^{(3)}$ values were obtained for different concentrations, suggesting strong molecular aggregation effects. The $\chi^{(3)}$ values obtained for our composite samples are in rough agreement with the predictions of a simple additive model based on non-interacting Pc molecules, assuming $\gamma = 3.9 \times 10^{-32}$ esu, as measured by EFISH (Electric Field Induced Second Harmonic) at the same wavelength.[126] In contrast, such concentrations either in spin-coated or evaporated films reduce the non-linear response associated with each molecule.[127]

The non-linear absorption dispersion was studied by Z-scan.[128] This technique measures the total laser energy transmitted through the sample. This is given as a sample position function along the optical axis with respect to the focal plane. The results indicate that the sign of the non-linear refractive index changes near 550 nm. However, to enhance the magnitude and spectral characteristics of the negative refractive index range in the composite, the processing should lead to a monomer/aggregate ratio that is as high as possible.

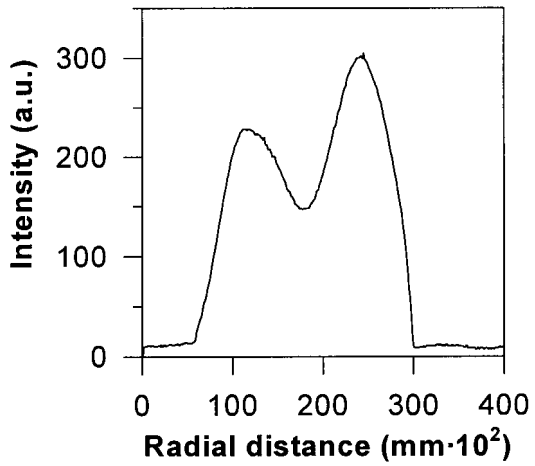

Figure 11 Intensity profile distortion of a gaussian laser beam 0.6 m after passage though a CuPc–sonogel composite (5×10^{-5} M CuPc concentration). Incident intensity on the sample was $I = 2.0 \times 105$ W m^{-2}.

4.2 Semiconductor-doped sonogels

The enhanced fine and uniform porosity and high mechanical stability of sono-xerogels obtained in the presence of DCCA suggested the potential to produce semiconductor dots by a sol–gel process in an inorganic matrix. Bagnall and Zarzycki obtained CdS_xSe_{1-x} precipitates in sonogel matrices prepared with DCCA[129] by chemical reaction in the interstitial liquid. They found that the lower diffusivity in sonogels, as compared with classic wet gels, enabled fine and uniform precipitates to be obtained. To optimize optical quality, an impregnation treatment using SiO_2 sonosols was developed,[130] reinforcing the matrix mechanical properties by sealing their pores. This allows perfectly smooth surfaces to be obtained after polishing.

Research on the preparation and characterization of quantum dots in silica sono-xerogels matrices has been described elsewhere.[68] Very fine CdSe[131] particles with a homogeneous size distribution were obtained by immersing Cd^{2+}-doped gels in a KSeCN solution. The UV–Vis absorption spectrum, at room temperature, is blue-shifted relative to the CdSe bulk absorption band position, a characteristic of the carrier confinement effect. The particle size and absorption threshold abide by the condition $\Delta E \propto 1/R^2$, R being the particle radius. Likewise, samples with CdS particles were prepared. Figure 12 is a high-resolution transmission electron microscope (HRTEM) image of a CdS/SiO_2 composite in which the crystalline structure of the semiconductor dots surrounded by the amorphous silica sonogel matrix can be observed. A higher dot population was achieved by the sonogel method than in standard alcohol solutions. This is indicated by the curve knee near a scattering vector modulus of 0.5 nm^{-1} in the SAXS intensities (Fig. 13).

Impurities or traps play an important role in the photoluminiscence yield. Traps are metastable states that capture electrons from higher-energy states, allowing ready transition to much lower-energy states.[132] When traps are localized at the matrix–semiconductor interface, the transition is not radiative, resulting in a photodarkening of the sample. The photoluminiscence yield of these quantum dots is shown in Fig. 14, featuring a narrow peak corresponding to the intrinsic band on the high-energy side and a broad peak at lower energies due to the defect traps on the crystal surface. As has been reported by Butty *et al.*,[133] the intrinsic band on the porous gel is not resolved, revealing the high quality of the crystal surfaces in CdS-doped sonogels as compared with the classic systems, probably due to the elimination of surface recombination sites.[134]

4.3 Ceramic–ceramic composites

Ceramic–ceramic composites can be prepared by the sol–gel processes by infiltration of a reinforcing phase with a low-viscosity sol. This method favors the formation of an intimate interface between the matrix and reinforcing phase after gelation, resulting in a high interfacial bond strength which should improve mechanical performance. The sonogel method offers the possibility of obtaining denser matrices with shorter, controllable, gelation times.

We have fabricated cordierite ($5SiO_2 \cdot 2Al_2O_3 \cdot 2MgO$) by the sonogel route and studied the effect of the addition of 7–15 mol% TiO_2 on the nucleation and crystallization processes. Highly homogenous ceramic–ceramic composites were obtained by mechanical dispersion of various reinforcing phases (ZrO_2 and Al_2O_3 short fibers with volume fractions varying from 0 to 0.6) in the matrix solution. After gelation, the composite preforms were dry-densified by hot-pressing at 1000 °C. Devitrification of sintered cordierite sonogels shows that, when the polymorphic crystalline μ- and α-cordierite forms appear, a substantial increase in mechanical strength is observed.[135]

ZrO_2 ceramic felts were also used to improve the

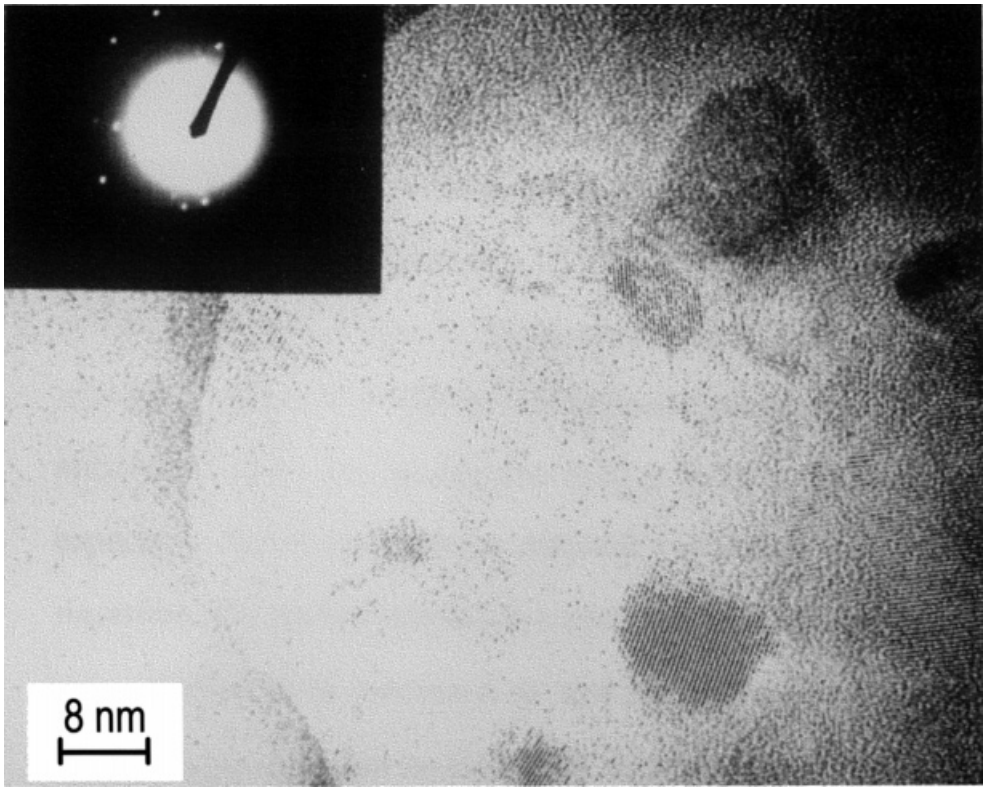

Figure 12 HRTEM micrograph of CdS quantum dots in a sono-xerogel matrix, showing the crystalline structure of the semiconductor dots surrounded by the amorphous matrix.

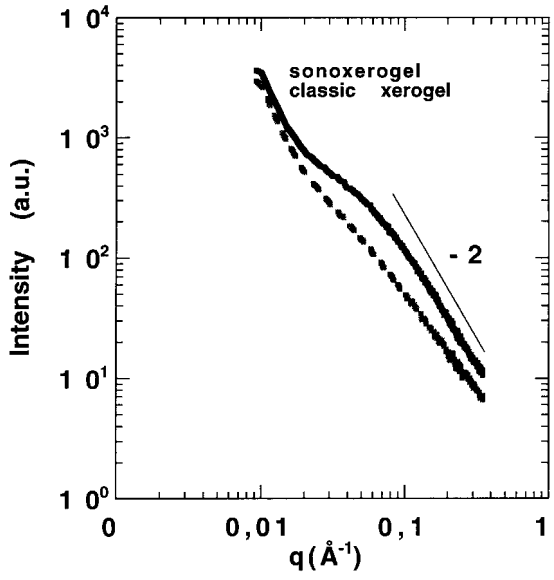

Figure 13 SAXS log–log curves of CdS-doped sono- and classic xerogels.

mechanical properties of cordierite. These samples were sintered by hot-pressing of several impregnated ZrO_2 felt layers at 900 °C. Relative densities were around 90% and the rupture moduli were around 150 MPa.[136] Scanning electron micrographs (SEMs) at different steps in the process are shown in Fig. 15.

The mechanical behavior and thermal properties of these composites were studied as a function of the volume fraction of the inclusions and sintering temperature. Mechanical testing and SEM analysis showed that both bending strength and elastic modulus decreased for higher fiber concentrations as a consequence of the slight porosity created by mismatched expansion between matrix and fibers, imperfections and discontinuities appearing along the matrix–fiber interface.[137] The maximum values were 97.1 MPa and 43.3 GPa, respectively, achieved with a 0.2 volume fraction of fibers. Indentation studies indicated a toughening mechanism of the matrix caused by the inclusions which leads to higher K_{IC} values, from 1.20 to 2.66 MPa $m^{1/2}$.

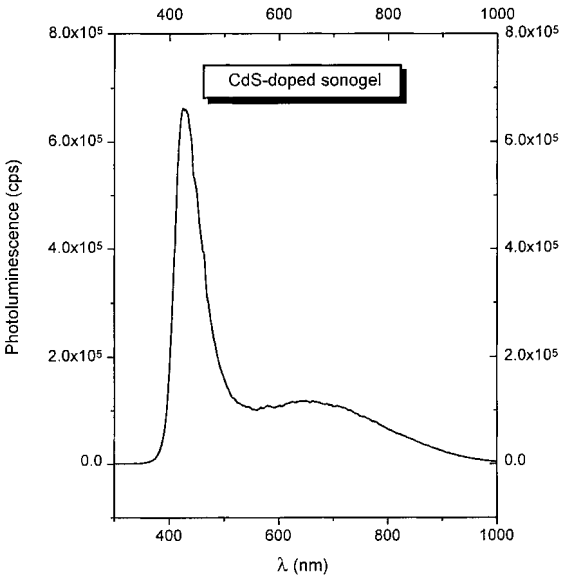

Figure 14 Photoluminiscence spectra of CdS quantum dots in a silica sonogel matrix at 300 K. The excitation intensity was about 2 MW cm^{-2} at a wavelength of 355 nm, with a 6 ns pulse duration from a Q-switch Nd:YAG laser.

4.4 Catalysts

The preparation of materials by sol–gel methods is used extensively in catalysis production, as detailed in reviews.[138,139] The possibility of controlling the composition, texture and structure of nanostructured phases by sol–gel synthesis provides the potential to modulate the catalytic behavior of the resulting solids. The role of ultrasound as an external agent to improve the catalyst surface chemical properties has been described recently by Suslick.[140] Improvements can be induced through the use of ultrasound during catalyst preparation (sonogel), which is the object of the present review, or alternatively through its direct action under catalysis conditions.

Cauqui and co-workers[58,141–145] reported the modulation of the textural properties of TiO_2–SiO_2phases, with TiO_2 content ranging from 0 to 10 mole%, as a catalyst or catalytic support. When dealing with supercritically dried sonogels, they found that after a prolonged calcination treatment in flowing oxygen or flowing hydrogen up to 1073 K the specific surface area remained well above 700 $m^2 g^{-1}$.[58,141,144]

Chemical characterization studies show that the use of ultrasound to prepare supports also contributed to improve dispersion of titanium in the silica network.[144] This conclusion was reached from reaction studies that monitored acid sites generated by Ti–O–Si sites. Their classic counter-

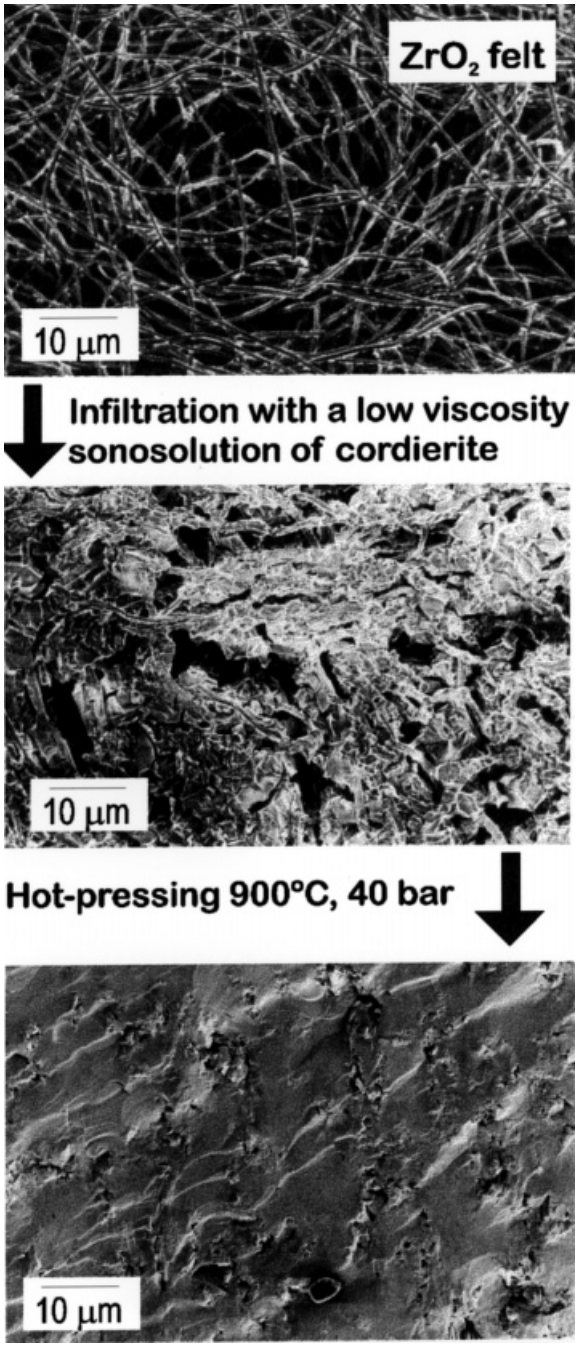

Figure 15 SEM micrographs taken at different stages during the fabrication process of composites by infiltration of a ZrO_2 ceramic felt with cordierite sols.

parts undergo chemical changes in the wet starting gels.[58,144] It appears that the pressure and temperature conditions used during drying can induce a selective chemical dissolution of titanium species, which then reprecipitate as anatase patches. Another surprising fact is the lack of microporosity in the titania–silica sono-aerogels.[58] However, in an analogous series of sono-xerogels, the titanium dispersion in the network remains high, although a significant contribution from micropores is unavoidable.[141]

When dried sonogels are impregnated with metal salt solutions to obtain dispersed active metal catalysts, the systems must be dried again. If this second drying is carried out conventionally, the pore structure of the sample suffers from capillary stress. However, the gels are stiff enough to moderate sintering associated with this type of impregnation process. According to the literature,[141,142,144] the specific surface area of supported metal catalysts prepared by impregnation remains greater than 500 $m^2 g^{-1}$.

The procedure described above was followed to prepare supported metal catalysts of rhodium,[141,142,145] nickel[142,145] and platinum.[144,145] In all cases the dispersion in sonogel catalysts was higher or equivalent to in classic gels. Benzene hydrogenation and butane hydrogenolysis were studied as test reactions using the prepared catalysts. As a general trend in these reactions, the activities and selectivities of sono-aerogel supported catalysts were higher than those supported on classic gels. The sono-obtained catalysts deactivate more slowly, a very important point for prospective applications. It is also worthy of mention that the classic aerogels gave catalytic properties superior to reference catalysts of similar composition prepared using commercial supports.

Another interesting point is that the sonogel catalysts did not show the typical inhibition of activity with increases in the reduction temperature, reported as a strong metal–support interaction (SMSI) effect.[141] This effect is observed for titania-silica samples of similar composition prepared by conventional routes without sol–gel supports. In contrast, increases in benzene hydrogenation activity in parallel with the reduction temperature were found, and attributed to a different kind of metal–support interaction. Thus, the chemistry of the gel support stabilizes the activity of the catalyst with time, and induces favorable metal–support interactions.

An alternative way of incorporating metals into the catalyst is by adding a metal precursor salt during the gelling process.[145,146] This makes it even more difficult to understand the details of the chemical processes that operate during gel formation. In these cases, the available reports suggest that the selection of the metal precursor plays a crucial role in determining the final metallic dispersion. Thus Cauqui *et al.*[141] did not succeed in obtaining a good dispersion for rhodium. Nevertheless, the catalyst obtained showed a very high ability to absorb hydrogen by a spill-over mechanism.

Finally, we should mention characterization[146,147] for Pt catalysts prepared with silica sonogels as supports; the authors concluded that the method followed for the preparation determines the surface acidic properties of the catalysts, thus modulating their catalytic behavior.

TiO_2–SiO_2 gels can be used as catalyst supports for SMSI[148] catalysts. The inclusion of titania in a silica sono-aerogel matrix restrains the migration of titania and inhibits the coverage of the metal particle by support species, leading to catalysts with improved activities. When the metal (rhodium) is introduced during the hydrolysis stages of the preparation of a titania-doped silica sonogel, X–O–Rh bonds are formed which favor the adsorption of large amounts of hydrogen, at room temperature, by a spill-over process. This suggest a new type of metal–support interaction.

REFERENCES

1. H. Dislich, *Angew. Chem. Int. Ed. Engl.* **10**, 363 (1971).
2. R. Roy, *J. Am. Ceram. Soc.* **52**, 344 (1969).
3. D. R. Secrist, and J. D. Mackenzie, *Mod. Asp. Vitr. State* **3**, 149 (1964).
4. Sol–Gel Processes for Ceramic Nuclear Fuels, Proc. of a Panel sponsored by IAEA, Vienna, 6–10 May 1968.
5. Symp. on Sol–Gel Processes and Reactor Fuel Cycles, Gatlinburg, USA, 4–7 May 1970, Conf. 700502.
6. Sol–Gel Processes for Fuel Fabrication, Proc. Panel organized by IAEA, Vienna, 21–24 May 1973, IAEA-161.
7. L. L. Hench, and J. K. West, *Chem. Rev.* **90**, 33 (1990).
8. D. R. Ulrich, *J. Non-Cryst. Solids* **100**, 174 (1988).
9. J. D. Mackenzie, *J. Non-Cryst. Solids* **41**, 1 (1982).
10. S. Sakka, and K. J. Kamiya, *J. Non-Cryst. Solids* **42**, 403 (1980).
11. H. Dislich, *J. Non-Cryst. Solids* **73**, 599 (1985).
12. M. Yamane, S. Aso, and T. Sakaino, *J. Mater. Sci.* **13**, 865 (1978).
13. C. J. Brinker, and G. W. Scherer, *Sol Gel Science*, Academic Press, San Diego, 1990.

14. J. T. Davis, and E. K. Rideal, *Interfacial Phenomena*, Academic Press, New York, 1963.
15. P. J. Flory, *Faraday Disc. Chem. Soc.* **57**, 7 (1974).
16. E. M. Rabinovich, in *Sol–gel Technology for Thin Films, Fibers, Preforms, Electronics and Special Shapes*, Klein, L. C. (ed), Noyes, Park Ridge, NJ, 1988, pp. 260–294.
17. L. L. Hench, in *Science of Ceramic Chemical Processing*. L. Hench and D. R. Ulrich (eds), Wiley, New York, 1986, p. 52.
18. M. Ramírez-del-Solar, L. Esquivias, A. F. Craievich, and J. Zarzycki, *J. Non-Cryst. Solids* **147–148**, 206 (1992).
19. J. Zarzycki, in *Chemical Processing of Advanced Materials*, L. Hench and J. K. West (eds), John Wiley, New York, 1992, p. 84.
20. J. Zarzycki, *J. Non-Cryst. Solids* **147–148**, 176 (1992).
21. J. Rodríguez Ortega, Ph. D. Thesis, University of Cádiz, 1996.
22. J. Rodríguez Ortega, and L. Esquivias, *J. Sol–Gel Sci. Technol* **8**, 117 (1997).
23. E. Blanco, N. de la Rosa-Fox, L. Esquivias, and A. F. Craievich, *J. Non-Cryst. Solids* **147–148**, 296 (1992).
24. S. S. Kistler, *J. Phys.Chem.* **36**, 52 (1932).
25. G. A. Nicolaon, and S. J. Teichner, *Bull. Soc. Chim. Fr*. 1900 (1968).
26. M. Prassas, Ph. D. Thesis, University of Montpellier II, 1981.
27. J. Zarzycki, M. Prassas, and J. Phallipou, *J. Mater. Sci.* **17**, 3371 (1982).
28. M. Prassas, J. Phallipou, and J. Zarzycki, *J. Phys. C-9* **43**, 257 (1982).
29. J. Phalippou, T. Woignier, and J. Zarzycki, in *Ultrastructure Processing of Ceramics, Glasses and Composites*, Ulhmann, D. R. and Ulrich, D. R. (eds), Wiley–Interscience, New York 1984, pp. 70–87.
30. T. Woignier, Ph. D. Thesis, University of Montpellier II, 1984.
31. J. Fricke (ed.), *Aerogels,. Pro. 1st Int. Symp. on Aerogels (ISA1)*, Springer-Verlag, Berlin, 1986; R. Vacher, J. Phalippou, J. Pelous, T. Woignier, (Guest eds), *Proc. ISA2, J. Phys. App.* **4** (supplement) (1989), J. Fricke, (Guest eds), *Proc. ISA3, J. Non-Cryst. Solids* **145**, (1992); R. W. Pekal, L. W. Hrubesch, (Guest eds), *Proc. ISA 4, J. Non-Cryst. Solids* **186**, (1995).
32. J. Zarzycki, *J. Non-Cryst. Solids* **121**, (1990).
33. J. Fricke (ed), *Aerogels, Springer Proc. Physics*, Vol. 6, Springer, Heidelberg, 1986.
34. J. Fricke, and A. Emmerling, in *Aerogels- Preparation, Properties, Applications* Resifeld, R. and Jøergensen, (eds), *Springer Ser. Structure and Bonding*. Vol. 177, Springer, Heidelberg, 1992, p. 37.
35. J. Fricke, *J. Non-Cryst. Solids* **147–148**, 356 (1992).
36. B. Fegley, P. White, and H. K. Bowen, *Am. Ceram. Soc. Bull* **64**, 1115 (1985).
37. S. Sakka, and K. Kamiya, *J. Non-Cryst. Solids* **48**, 31 (1982).
38. T. Yoko, and S. Sakka, *J. Non-Cryst. Solids* **147–148**, 394 (1992).
39. J. Zarzycki, in *Glass: Science and Technology*, Vol. 2 Ulhmann, D. R. and Kreidl, N. J. (eds), Academic Press, Orlando, 1984, pp. 209–249.
40. M. Tarasevich, *Cer. Bull.* **63**, 500 (1984) (abstract only).
41. J. Zarzycki, *Heterogen. Chem. Rev.* **1**, 243 (1994).
42. L. Esquivias, and J. Zarzycki, in *Current Topics on Non Crystalline Solids*, Baró, M. D. and Clavaguera, N. (eds), World Scientific, Singapore, 1986, pp. 409–414.
43. L. Esquivias, and J. Zarzycki, in *Ultrastructure Processing of Ceramics, Glasses and Composites*, Mackenzie, J. D. and Ulrich, D. R. (eds) Wiley, New York, 1988, pp. 255–270.
44. N. de la Rosa-Fox, L. Esquivias, and J. Zarzycki, *Diffusion and Defect Data* **53–54**, 363 (1987).
45. N. de la Rosa-Fox, L. Esquivias, and J. Zarzycki, *Rev. Phys. Appl.* **24**(4), 233 (1989).
46. M. Ramírez-del-Solar, N. de la Rosa-Fox, L. Esquivias, and J. Zarzycki, *J. Non-Cryst. Solids* **121**, 40 (1990).
47. N. de la Rosa-Fox, L. Esquivias, A. F. Craievich, and J. Zarzycki, *J. Non-Cryst. Solids* **192**, 211 (1987).
48. N. de la Rosa-Fox, L. Esquivias, and J. Zarzycki, *J. Mater. Sci. Lett.* **10**, 1237 (1991).
49. J. Zarzycki, in *Ultrastructure Processing of Advanced Materials*, Ulmann, D. R. and Ulrich, D. R. (eds), Wiley, New York, 1992, pp. 135–148.
50. C. Barrera-Solano, N. de la Rosa-Fox, and L. Esquivias, *J. Non-Cryst. Solids* **147–148**, 194 (1992).
51. M. Atik, Ph. D. Thesis, University of Montpellier II, 1990.
52. C. Fernández-Lorenzo, Ph. D. Thesis, University of Cadiz 1993.
53. C. Fernández-Lorenzo, L. Esquivias, P. Barboux, J. Maquet, and F. Taulelle, *J. Non-Cryst. Solids* **176**, 189 (1994).
54. M. Ramírez-del-Solar, Ph. D. Thesis, University of Cadiz 1991.
55. M. Ramírez-del-Solar, N. de la Rosa-Fox, L. Esquivias, and J. Zarzycki, *J. Non-Cryst. Solids* **121**, 84 (1990).
56. M. Ramírez-del-Solar, and L. Esquivias, *J. Sol–Gel Sci. Technol* **3** (1), 41 (1994).
57. J. M. Ruiz-Rube, M. Ramírez-del-Solar, N. de la Rosa-Fox, and L. Esquivias, in *Basic Features of the Glassy State*, Colmenero, J. and Alegría, A. (eds), World Scientific, Singapore, 1990, pp. 68–72.
58. J. J. Calvino, M. A. Cauqui, G. Cifredo, L. Esquivias, J. A. Pérez, M. Ramírez-del-Solar, and J. M. Rodríguez-Izquierdo, *J. Maer. Sci.* **28**, 2191 (1993).
59. L. Esquivias, and M. Ramírez-del-Solar, *J. Non-Cryst. Solids* **220** (1), 45–51 (1997).
60. D. Chaumont, A. F. Craievich, and J. Zarzycki, *J. Non-Cryst. Solids* **147–148**, 41 (1992).
61. D. Chaumont, Ph. D. Thesis, University of Montpellier II, 1992.
62. M. Piñero, M. Atik, and J. Zarzycki, *J. Non-Cryst. Solids* **192**, 523 (1987).
63. M. Piñero, Ph. D. Thesis, University of Cádiz, 1993.
64. K. Morita, Y. Hu, and J. D. Mackenzie, in *Mater. Res. Soc. Symp. Proc.* Vol. **271**, Materials Research Society, Pittsburgh, PA, 1992, pp. 693–698.
65. K. Morita, Y. Hu, and J. D. Mackenzie, *J. Sol–Gel Sci. Technol.* **3**, 109 (1994).

66. T. Iwamoto, and J. D. Mackenzie, *J. Sol–Gel Sci. Technol.* **4**, 141 (1995).
67. M. Piñero, and J. Zarzycki, *J. Sol–Gel Sci. Technol.* **1**, 275 (1994).
68. M. Piñero, L. Litrán, C. Fernández-Lorenzo, E. Blanco, M. Ramírez-del-Solar, N. de la Rosa-Fox, L. Esquivias, A. F. Craievich, and J. Zarzycki, *J. Sol–Gel Sci. Technol.* **2**, 689 (1994).
69. E. Blanco, L. Litrán, M. Ramírez-del-Solar, N. de la Rosa-Fox, and L. Esquivias, *J. Mater. Res.* **9–11**, 2873 (1994).
70. A. F. Craievich, N. de la Rosa-Fox, E. Blanco, M. Piñero, M. Ramírez-del-Solar, and L. Esquivias, *NanoStruct. Mater.* **5**(3), 363 (1995).
71. D. C. Hummel, I. L. Torriani, A. Y. Ramos, A. F. Craievich, N. de la Rosa-Fox, and L. Esquivias, in *Mater. Res. Soc. Symp. Proc.* Vol **246**, Materials Research Society Pittsburgh, PA, 1994, pp. 673–678.
72. L. Litrán, M. Ramírez-del-Solar, E. Blanco, N. de la Rosa-Fox, and L. Esquivias, in *Nanostructured and Non-Crystalline Solids*, Vázquez, M. and Hernando, A. (eds), World Scientific Singapore, 1995, pp. 109–113.
73. R. Litrán, E. Blanco, M. Ramírez-del-Solar, and L. Esquivias, *J. Sol-Gel Sci. Technol.* **8**(1–3), 985 (1997).
74. L. Litrán, P. M. Petersen, P. M. Johansen, L. Linvold, M. Ramírez-del-Solar, and E. Blanco, *J. Appl. Phys.* **81**, 7728 (1997).
75. P. M. Petersen, L. Litrán, P. M. Johansen, and L. Lindvold, *SPIE Proc.* **2788**, 202 (1996).
76. L. Litrán, E. Blanco, M. Ramírez-del-Solar, A. Hierro, M. A. Díaz-García, A. García-Cabañes, and F. Agulló-López, *Synth. Met.* **83**, 273 (1997).
77. J. I. S. Zink, A. Yamanaka, L. M. Ellerby, J. S. Valentine, F. Noshida, and B. Dunn, *J. Sol–Gel Sci. Technol.* **2**, 791 (1994).
78. D. Avnir, and V. R. Kaufman, *J. Non-Cryst. Solids* **192**, 180 (1987).
79. J. W. Flemming, and S. A. Flemming, Vapogel as new glass-forming technique, Paper presented at Materials Res. Soc. meeting, 5–9 April 1988, Reno, NV.
80. W. M. Jones, and D. B. Fischbach, *J. Non Cryst. Solids* **101**, 123 (1988).
81. G. Kundu, B. Karmakar, and D. Ganguli, *J. Non-Cryst. Solids* **122**, 219 (1990).
82. K. G. Sharp, *J. Sol–Gel Sci. Technol.* **2**, 35 (1994).
83. P. D. Fuqua, K. Mansour, D. Álvarez Jr., S. R. Marder, J. W. Perry, and B. Dunn, Synthesis and nonlinear optical properties of sol–gel materials containing phthalocyanines. In *SPIE 1758, Sol–Gel Optics II*, 499–506 (1992).
84. J. P. Lorimer, and T. J. Mason, *Chem. Soc. Rev.* **16**, 239 (1987).
85. E. A. Neppiras, *Ultrasonics* **22**(1), 25 (1984).
86. M. E. Fitzgerald, V. Griffing, and J. Sullivan, *J. Chem. Phys.* **25**, 926 (1974).
87. B. E. Nolting, and E. A. Nepiras, *Proc. Phys. Soc. B* **63**, 674 (1950).
88. D. J. Donalson, M. D. Farrington, and P. Kruss, *J. Phys. Chem.* **83**, 3130 (1979).
89. E. C. Couppis, and G. E. Klinzing, *AIChE J.* **20**(3), 485 (1974).
90. F. G. P. Aerstin, K. D. Timmerhaus, and H. S. Fogler, *AIChE J.* **13**(3), 453 (1967).
91. J. C. Pouxviel, J. P. Boilot, J. C. Beloeil, and Y. Lallemand, *J. Non-Cryst. Solids* **89**, 345 (1987).
92. G. Orcel, and L. Hench, *J. Non-Cryst. Solids* **79**, 177 (1986).
93. D. A. Donatti, and D. R. Vollet, *J. Sol–Gel Sci. Technol.* **4**, 99 (1995).
94. D. R. Vollet, D. A. Donatti, and J. R. Campanha, *J. Sol–Gel Sci. Technol.* **6**, 57 (1996).
95. J. Jonas, A. D. Irwin, and J. S. Holmgen, in: *Ultrastructure Processing of Advanced Ceramics*, Mackenzie J. D. and Ulrich, D. R. (eds). Wiley, New York, 1990, p. 303.
96. A. Pérez-Moreno, C. Jiménez-Solís, L. Esquivias, and N. de la Rosa-Fox, *Paper presented at the Bienal de la Sociedad Española de Cerámica y Vidrio*, San Sebastián, Spain, 1996.
97. W. Wei, *J. Non-Cryst. Solids* **81**, 239 (1986).
98. A. B. Rosenthal, and S. Garofalini, *J. Non-Cryst Solids* **107**, 65 (1988).
99. B. E. Warren, *in X-ray Diffraction*, Addison-Wesley, New York, 1969.
100. O. Glatter, and O. Kratky, *Small Angle X-Ray Scattering*, Academic Press, London, 1982.
101. B. H. Zimm, *J. Chem. Phys.* **16**, 1093 (1948).
102. D. W. Schaefer, *Mater. Res. Soc. Bull.* **8**, 22 (1988).
103. N. de la Rosa-Fox, L. Esquivias, A. Craievich, and J. Zarzycki, *J. Non-Cryst. Solids* **121**, 211 (1990).
104. S. Doeuff, M. Henry, C. Sánchez, and J. Livage, *J. Non-Cryst. Solids* **89**, 206 (1987).
105. C. J. Brinker, K. D. Keefer, D. W. Schaefer, R. A. Assink, B. D. Kay, and C. S. Ashley, *J. Non-Cryst. Solids* **63**, 45 (1984).
106. G. Philipp, and H. Schmidt, *J. Non-Cryst. Solids* **63**, 283 (1984).
107. G. Wilkes, B. Orler, and H. Huang, *Polym. Prepr.* **26**(2), 47 (1985).
108. H. Huang, B. Orler, and G. L. Wilkes, *Polym. Bull.* **14**, 557 (1985).
109. H. J. Schmidt, *Non-Cryst. Solids* **73**, 681 (1985).
110. B. K. Coltrain, C. Sánchez, D. W. Schaefer, and G. L. Wilkes, Better Ceramics Through Chemistry VII: Organic/Inorganic Hybrid Materials, MRS Symp. Proc. Vol. 435, Materials Research Society, Pittsburgh, PA, 1996.
111. L. Klein, and C. Sánchez, *Organic/Inorganic Hybrid Materials, J. Sol–Gel Sci. Technol.* **5**(2), (1995) and **7**(3), (1996) (special issues).
112. J. D. Mackenzie, *J. Sol-Gel Sci. Technol.* **2**, 81 (1994).
113. E. J. A. Pope, and J. D. Mackenzie, *MRS Bull.* **17**, 29 (1987).
114. H. Huang, B. Orler, and G. L. Wilkes, *Macromolecules* **20**, 1322 (1987).
115. J. D. Mackenzie, Y. J. Chung, and Y. Hu, *J. Non-Cryst. Solids* **147–148**, 271 (1992).
116. D. Avnir, D. Levy, and R. Reisfeld, *J. Phys. Chem.* **88**, 5956 (1984).
117. D. Levy, and D. Avnir, *J. Phys. Chem.* **92**, 4734 (1988).
118. E. Blanco, M. García-Hernández, R. Jiménez-Riobóo, L. Litrán, C. Prieto, and M. Ramírez-del-Solar, Paper

presented at the 9th Int. Workshop on Glasses and Ceramics from Gels, 1–5 Sept 1997, Sheffield, UK.
119. Y. Hu, and J. D. Mackenzie, *J. Mater. Sci.* **27**, 4415 (1992) and references therein.
120. M. García-Hernández, R. Jiménez-Riobóo, C. Prieto, J. J. Fuentes-Gallego, E. Blanco, and M. Ramírez-del-Solar, *Appl. Phys. Lett.* **69**, 3827 (1996).
121. R. Jiménez-Riobóo, M. García-Hernández, C. Prieto, J. J. Fuentes-Gallego, E. Blanco, and M. Ramírez del Solar, *J. Appl. Phys.* **81**, 7739 (1997).
122. M. Canva, P. Georges, G. Le Saux, A. Brun, D. Larrue, and J. Zarzycki, *J. Mater. Sci. Lett.* **10**, 615 (1991).
123. M. Canva, P. Georges, A. Brun, D. Larrue, and J. Zarzycki, *J. Non-Cryst. Solids* **147–148**, 627 (1992).
124. D. Dolphin (ed.), *The porphyrins*, Vols 1–7, Academic Press, New York, 1978–1979.
125. F. Kajzar, and J. Messier, in *Nonlinear Optical Properties of Organic Molecules and Crystals*, Vol. 2, Chemla, D. S. and Zyss, J. (eds), Academic Press, New York, 1987, p. 51.
126. M. A. Díaz-García, I. Ledoux, J. A. Duro, T. Torres, F. Agulló-López, and J. Zyss, *J. Phys. Chem.* **98**, 8761 (1994).
127. M. A. Díaz-García, F. Agulló-López, W. E. Torruellas, and G. I. Stegman, *Chem Phys. Lett.* **235**, 535 (1995).
128. E. Blanco, D. Narayana Rao, F. J. Aranda, D. V. G. L. N. Rao, S. Tripathy, R. Litrán, and M. Ramírez-del-Solar, *J. Appl. Phys.* **83**(3), (1998) (in the press).
129. C. Bagnall, and J. Zarzycki, *SPIE Proc. Sol–Gel Optics I*, **108**, 1328 (1990).
130. M. Canva, P. Georges, G. LeSaux, A. Brun, D. Larrue, and J. Zarzycki, *J. Non-Cryst. Solids* **147–148**, 636 (1992).
131. D. Hummel, I. L. Torriani, A. Y. Ramos, A. F. Craievich, N. de la Rosa-Fox, and L. Esquivias, in *Better Ceramics Through Chemistry V*, Sanchez, C. (ed.) Materials Research Society, Pittsburgh, PA, 1994, pp. 673–678.
132. J. I. Pankove, *Optical Processes in Semiconductors*, Dover, New York, 1971, p. 370.
133. J. Butty, N. Peyghambarian, Y. H. Kao, and J. D. Mackenzie, *Appl. Phys Lett.* **69**(21), 3224 (1996).
134. N. de la Rosa-Fox, M. Pinero, R. Litrain, and L. Esquivias, presented at Sol-Gel '99, September 19–24, 1999, Yokohama, USA.
135. M. Piñero, M. Atik, and J. Zarzycki, *J. Non-Cryst. Solids* **147–148**, 523 (1992).
136. M. Piñero, and J. Zarzycki, *J. Sol-Gel Sci. Technol*, **1**, 275 (1994).
137. M. Piñero, C. C. Barrera-Solano, C. Jiménez-Solís, L. Esquivias, and J. Zarzycki, in *Advances in Ceramic–Matrix Composites III*, Narottam, P. Bansal, J. P. and Singh (eds), American Ceramic Society, Indianápolis, 1996, p. 471.
138. G. M. Pajonk, *Appl. Catal.* **72**, 217 (1991).
139. M. A. Cauqui, and J. M. Rodríguez-Izquierdo, *J. Non-Cryst. Solids* **147–148**, 724 (1992).
140. K. S. Suslick, Sonocatalysis. in *Handbook of Heterogeneous Catalysis*, Ertl, G. Knözinger, H. and Weitkamp, J. (eds), VCH Weisheim, 1997, pp. 1350–1357.
141. M. A. Cauqui, J. J. Calvino, G. Cifredo, L. Esquivias, J. A. Pérez, and J. M. Rodríguez-Izquierdo, *J. Non-Cryst. Solids* **147–148**, 758 (1992).
142. J. J. Calvino, M. A. Cauqui, G. Cifredo, J. M. Rodríguez-Izquierdo, and H. Vidal, *J. Sol–Gel Sci. Technol.* **2**, 831 (1994).
143. J. J. Calvino, M. A. Cauqui, J. M. Gatica, J. A. Pérez, and J. M. Rodríguez-Izquierdo, *Mater. Res. Soc. Symp. Proc.* **346**, 685 (1994).
144. S. Bernal, J. J. Calvino, M. A. Cauqui, J. M. Rodríguez-Izquierdo, and H. Vidal, *Stud. Surf. Sci. Catal.* **91**, 461 (1995).
145. M. A. Cauqui, Doctoral Thesis, University of Cadiz, 1994.
146. T. López, M. Asomoza, R. Gómez, P. Bosch, J. M. Rodríguez-Izquierdo, and M. A. Cauqui, *Thermochim. Acta.* **255**, 319 (1995).
147. P. Bosch, T. López, M. Asamoza, R. Gómez, M. A. Cauqui, and J. M. Rodríguez-Izquierdo, *Langmuir* **11**, 4328 (1995).
148. J. J. Calvino, M. A. Cauqui, L. Esquivias, J. A. Pèrez, M. Ramirez-del-Solar, and J. M. Rodríguez-Izquierdo, *J. Mater. Sci.* **28**, 2191–2195 (1985).

